IEEE Access
Multidisciplinary | Rapid Review | Open Access Journal

Received January 27, 2020, accepted February 10, 2020, date of publication February 14, 2020, date of current version February 27, 2020.

Digital Object Identifier 10.1109/ACCESS.2020.2974003

Exploring the Information Capacity of Remote Sensing Satellite Networks

RUNZI LIU[1,2], (Member, IEEE), WEIHUA WU[3], QINGHAI YANG[3], DI ZHOU[3], AND WENZHU ZHANG[1]

[1]School of Information and Control Engineering, Xi'an University of Architecture and Technology, Xi'an 710055, China
[2]Science and Technology on Communication Networks Laboratory, The 54th Research Institute of CETC, Shijiazhuang 050081, China
[3]State Key Laboratory of ISN, School of Telecommunications Engineering, Xidian University, Xi'an 710071, China

Corresponding author: Weihua Wu (whwu@xidian.edu.cn)

This work was supported in part by the National Natural Science Foundation of China under Grant 61701365, Grant 61801365, Grant 61971327, and Grant 91338114, in part by the China Postdoctoral Science Foundation under Grant 2018M643581 and Grant 2019TQ0241, in part by the National Natural Science Foundation of Shaanxi Province under Grant 2019JQ-152, in part by the Postdoctoral Foundation in Shaanxi Province of China, and in part by the Fundamental Research Funds for the Central Universities.

ABSTRACT With the increasing demand for geological and weather information, remote sensing satellite networks (RSSNs) play increasingly important roles in monitoring our planet. On account of the significant differences between RSSNs and traditional communication networks, the traditional communication capacity which only focus on the performance of data transmission process cannot well capture the service capability of RSSNs. In order to provide efficient guidelines to the deployment of RSSNs, in this paper we study a new capacity indicator, called information capacity, which takes into account the whole service process of RSSNs, including information acquisition, processing, storage, and transmission. Specifically, we firstly propose the formal definition of information capacity. Then, a new graph model called microscopic time-expanded graph (MTEG) is developed, which characterizes the intertwined impact of the observation, computational, storage and transmission resources on the service process of RSSNs. Base on this graph model, a mathematical framework is developed to compute the information capacity. Owing to the NP-completeness of the formulated problem, we decompose it into a flow optimization problem and an arc scheduling problem of the MTEG model, and then propose a Graph-based Information Capacity Solving (GICS) algorithm to efficiently solve the problem. Finally, simulation results highlight the necessity of study the information capacity of RSSNs.

INDEX TERMS Remote sensing satellite networks, network capacity, performance analysis.

I. INTRODUCTION

Remote sensing is the technique of deriving information about objects or phenomena remotely without physical contact with them [1]. Benefiting from the extensive coverage, remote sensing satellites have become important participants in earth observation, and the acquired data of them are of great need in the study of climate change, environment protection, disaster control and so on. To meet with the surging volume and real-time requirements of geological information, more and more remote sensing satellites are launched to form constellation and networks in past decades [2]. Thus, the analysis and investigation of remote sensing satellite networks (RSSNs) has become a hot topic in the field of space research and design [3], [4].

Network capacity is one of the most prominent metrics to characterize the network performance. The capacity of terrestrial networks has been widely studied [5]–[7] since the seminal work of Kumar in 2000 [8]. In these works the capacity is described as the maximum achievable throughput of the network. Similarly, in [9], [10] the authors study two-layered satellite networks, wherein the capacity is defined as the maximum achievable throughput of the network. In [11], [12], the authors investigate the communication capacity of space-ground networks, which is defined as maximum total amount of data downloaded to the ground per unit time. In above literatures, the capacity defined based on throughput can well capture the service capability of networks.

The associate editor coordinating the review of this manuscript and approving it for publication was Antonino Orsino.

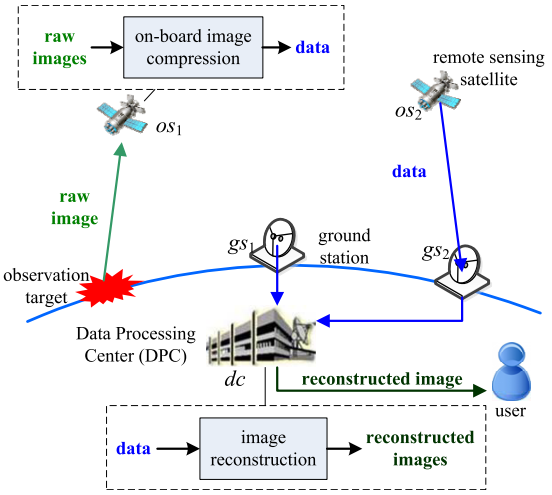

FIGURE 1. An example remote sensing satellite network.

However, the *throughput-based capacity* can not work well in RSSNs, due to the remarkable differences between RSSNs and traditional communication networks. Fig. 1 illustrates an example of service processing of RSSNs. It can be seen that firstly remote sensing satellites acquire raw images by imagers. Afterwards, the raw images are compressed by compression unit. Then, the compressed data will be transmitted to ground stations and finally sent to the Data Processing Center (DPC). After arriving at the DPC, the compressed images are reconstructed. At last, the reconstructed image is sent to the user. Based on the example, two major differences between RSSNs and traditional communication networks can be concluded.

- Besides the communication process, service capability of RSSNs is also impacted by information acquisition, processing and storage processes.
- Because of the effect of computational resources (e.g., compression unit), in RSSNs the amount of *effective information* delivered to the users per unit time is much more efficient to characterize performance than *throughput*.

Therefore, *a new metric should be considered to characterize the service capability of RSSNs*. As shown in Fig. 2, the new metric should cover the ensemble service process of RSSNs, which includes information acquisition, processing, storage, and transmission, rather than only takes the information transmission into account as the traditional throughput-based capacity. For the convenience of following discussion, the traditional throughput-based capacity is referred to as **communication capacity**, and the new indicator is referred to as **information capacity** hereinafter.

With the development of information technologies, the joint management of heterogenous resources, especially the 3C resources (i.e., Computing, Caching, and Communication resources), has become a new trend. Currently, some works focus on the joint optimization of multiple processes of information with different resources (especially information processing, storage and transmission) in terrestrial networks, such as internet of things [13], information centric networks [14] and mobile edge computing networks [15], [16]. However, it is still challenging to study the information capacity of RSSNs, due to several reasons: 1) Although there have been a big chunk of works focused on the capacity of networks, the indicator can efficiently characterize the capability to provide effective information to users of RSSNs is still absent. 2) On account of the compressing and reconstructing effect of computational resource, the data flows of RSSNs no longer keep conservation, which raises challenges to the analysis of information capacity. 3) The interactions among the information acquisition, processing, storage and transmission process is complex. For example, the observation and transmission processes of an agile remote sensing satellite[1] may conflict with each other when they require different attitude of satellite platform. Therefore, the service process of RSSNs cannot be resolve into independent parts to analysis respectively, so that it is essential to represent the observation, computational, storage and transmission resources jointly and characterize their intertwined impact the service process.

In this paper we explore the information capacity of RSSNs. We first propose the formal definition of information capacity. Then, we extend traditional time-expanded graph by modeling remote sensing satellite in a microscopic level and adding virtual arcs and virtual vertex. A new graph model called microscopic time-expanded graph (MTEG) is developed, which characterizes the intertwined impact of the information acquisition, processing, storage and transmission resources on the service process of RSSNs. Base on this graph model, we develop a mathematical framework to compute the information capacity. Owing to the NP-completeness of the formulated problem, we decompose it into a flow optimization problem and an arc scheduling problem of the MTEG model, and then propose a Graph-based Information Capacity Solving (GICS) algorithm to solve the problem in polynomial time. Simulation results highlight the necessity of study the information capacity of RSSNs.

The main contributions of this paper are as follows:

- To evaluate the service capability of RSSNs, we formally define a new indicator, information capacity, which involves the entire service processes.
- MTEG is developed to capture the time-varying coordination relationship among the observation, computational, storage and transmission resources and their intertwined impact on the service process in RSSNs.
- We formulate the problem of solving information capacity of RSSNs. Since the formulated problem falls in the category of mixed-integer nonlinear program (MINLP), we decompose it into a flow optimization problem and an arc scheduling problem based on the MTEG model. Then, a Graph-based Information Capacity

[1]An agile satellite is equipped with attitude and orbit control system (AOCS) to be able to turn around three axes: roll, pitch, and yaw. An example of an agile satellite is PLEIADES, which was developed by the CNES, the French Space Agency [17].

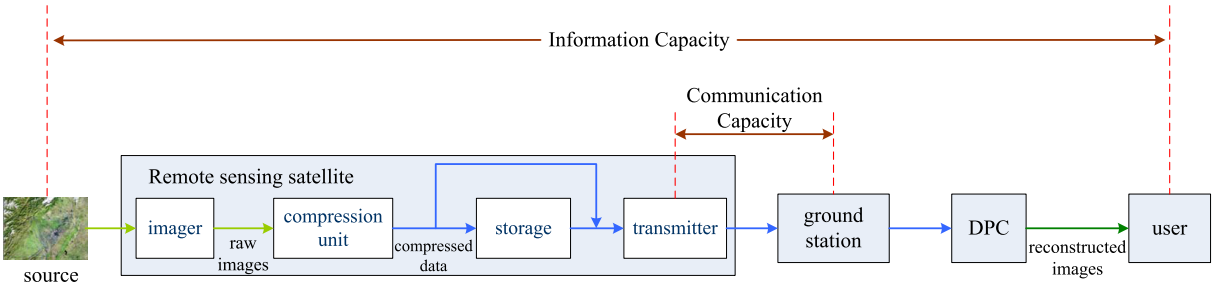

FIGURE 2. Comparison between information capacity and communication capacity. The light green, blue and dark green arrows indicate the flowing of raw images, compressed data and reconstructed images in RSSNs, respectively.

Solving (GICS) algorithm is proposed to efficiently solve the problem.
- Extensive simulation results are provided to validate the effectiveness and necessity of analysis of information capacity in RSSNs. The impacts of different network resources on the information capacity are evaluated.

The remainder of this paper is organized as follows. Section II introduces the RSSN system model under consideration and proposed the definition of information capacity of RSSNs. In Section III, we develop a graph model called microscopic time-expanded graph (MTEG) and formulate the problem of solving information capacity of RSSNs. Section IV decomposes the problem and then proposes a graph-based algorithm to solve the information capacity of RSSNs in polynomial time. The performance evaluation by simulations is presented in Section V, followed by concluding remarks in Section VI.

II. SYSTEM MODEL

A. NETWORK MODEL

Consider a remote sensing satellite network $\mathcal{N}$ (as illustrated in Fig. 1), which is comprised of:
- A set of remote sensing satellites, denoted by $OS = \{os_1, os_2, \ldots, os_n, \ldots\}$. The payloads of each remote sensing satellite include an imager, an image compression unit, a solid state mass storage and a transceiver.
- A set of ground stations $GS = \{gs_1, gs_2, \ldots, gs_n, \ldots\}$.
- A data processing center (DPC), denoted by dc.

During planning horizon $[0, T]$, there are a set of earth observation missions to be planed, which is denoted by $OM = \{om_1, om_2, \ldots, om_n, \ldots\}$. A mission om_j can be described by a 3-tuple $[ob_j, cr_j, dy_j]$, where ob_j denotes the observation target of mission om_j. Let $OB = \{ob_1, ob_2, \ldots, ob_n, \ldots\}$ denotes the set of observation targets in $\mathcal{N}$. cr_j denotes the maximum compression ratio that can be adopted by om_j. dy_j is the tolerable delay of om_j, which is the maximum length of time taken from image acquisition to arriving at the DPC.

RSSN completes the missions according to the plans provided by the Mission Operation Center (MOC). Fig. 2 illustrates the implementation process of a mission. Firstly, remote sensing satellites acquire the raw images of the observation target when it is in the observable range of the onboard imagers. Then, the raw images are encoded by the compression unit. Because of the orbiting movements, the link between a remote sensing satellite and a ground station can be established only when the satellite moves into the coverage of the ground station. That is to say, the compressed data are delivered to the ground station via store-carry-forward paradigm [18]. Therefore, the output of the compression unit would be stored in the onboard storage or transmitted directly. After arriving at the ground station, the compressed data are sent to the DPC and reconstructed. Finally, the reconstructed image is sent to the user.

Therefore, a mission plan should specify the remote sensing satellites and observation duration, compression level, the downlinks and the transmission duration for each mission. Moreover, to guarantee the QoS requirement of each mission, a feasible mission plan p should select a compression ratio no larger than cr_j for mission om_j and make all the image data be sent to the DPC within dy_j. Let P denote the set of feasible mission plans.

B. ONBOARD COMPUTATIONAL RESOURCES

Being capable of solving the "bandwidth vs. data volume" dilemma of modern spacecraft, onboard computational resource is playing a more and more vital role in the service of RSSNs. To be specific, with the growth of spatial resolution and swath of satellite imaging payloads, the ever increasing data acquisition rates incurs heavy burden on the limited on board communication and storage resources [19], [20]. For example, the acquisition data rate of CSG (COSMO-SkyMed Second Generation[2]) satellites can be up to 2×1.2 Gbit/s, while the data downlink rate and onboard storage capacity are only 2×260 Mbit/s and 1500 Gbit, respectively [21]. By compressing mission data, the onboard computational resources compensate for the limited onboard communication and storage resources, and thus improve the service capability of RSSNs effectively. However, there exist few works which focus on network capacity consider the effect

[2]COSMO-SkyMed second generation (Constellation of Small Satellites for Mediterranean basin observation) or CSG is an Earth observation program of the Italian Space Agency (ASI). The first satellite of CSG is scheduled to launch in the last quarter of 2019.

of computational resource. Therefore, in this subsection we propose the model of onboard computational resource.

With the development of onboard image compression algorithm and hardware design [22]–[24], the image compression module has become an indispensable payload of remote sensing satellites. For instance, the image compression module of CSG satellites can provide seven different compression ratios: 10:10 (uncompressed), 10:6, 10:5, 10:4, 10:3, 10:2 and 10:1. There are two classes of image compression methods: lossless or lossy [25]. With lossless image compression, the reconstructed image is exactly the same as the original one, without any information lost. On the contrary, lossy image compression would reconstruct the image with a varying degree of information loss. Generally, for a given lossy image compression method, the larger the compression ratio is, the more information is lost through compression.

In this paper, we assume each remote sensing satellite is equipped with an image compression module with processing rate R_p, which can provide Q levels of lossy compression.[3] Let $\varphi_i (1 \leq i \leq Q)$ denote the compression ratio of the ith level. Consider an $M \times N$ image with σ bit data quantization, where M and N are the number of rows and columns of pixels in the image. The original volume of this image is $MN\sigma$ bits. After the compression of ith level, only $\frac{MN\sigma}{\varphi_i}$ bits compressed data are required to be downloaded to the ground. At the DPC, an image of the same size with the original one can be reconstructed.

The distortion of a reconstructed image can be evaluated by image quality measures, such as Maximum Difference (MD), Peak Mean Square Error (PMSE), Normalized Mean Square Error (NMSE) [26]. Take NMSE as an example, which is defined as follows

$$NMSE = \frac{\sum_{j=1}^{M}\sum_{k=1}^{N}[F(j,k) - \hat{F}(j,k)]^2}{\sum_{j=1}^{M}\sum_{k=1}^{N}[F(j,k)]^2} \tag{1}$$

where $F(i,j)$ and $\hat{F}(i,j)$ denote the samples of original and reconstructed image. In this paper, we use the average NMSE of the images compressed by ith compression level, denoted by ds_i, to quantify the distortion caused by the ith compression level.

C. INFORMATION CAPACITY

In this subsection, we define a new metric called information capacity to capture the service capability of RSSNs. For the sake of convenience in comparison later, we first introduce the definition of communication capacity, before formally defining the information capacity.

Definition 1 (Communication Capacity [12]): The communication capacity of $\mathcal{N}$ is the maximum sum amount of the data that ground stations can receive from the satellites per unit time, i.e.,

$$C_{cm} = \frac{1}{T}\sum_{1\leq i\leq |OS|}\sum_{1\leq j\leq |GS|}\int_0^T \alpha_{ij}(t) r_{ij}(t) dt, \tag{2}$$

where $\alpha_{ij}(t)$ represents the availability of a link (the existence of a line-of-sight) between remote sensing satellite os_i and ground station gs_j, and $r_{ij}(t)$ denotes the data transfer rate between satellite os_i and ground station gs_j. □

As we have discussed in Section I, the major differences between communication capacity and information capacity lie in that communication capacity only focus on the information transmission process, while information capacity should cover the entire mission implementation process including information acquisition, processing, storage, and transmission. With the image compression and reconstruction of the information process, only the amount of data downloaded to the ground cannot reflect the service capability. To evaluate the information capacity of RSSNs, both the data volume and the quality of the images received by users should be taken into account. To this end, we define a metric, called *effective data volume*, to indicate the amount of valid information of a reconstructed image.

Definition 2 (Effective Data Volume): Consider an image which has been compressed under the ith level. After being reconstructed, the effective data volume of this image is

$$ed = rd \cdot (1 - ds_i), \tag{3}$$

where rd is the data volume of the reconstructed image. □

Thus, to measure the capability that RSSNs provide effective information to the users, the definition of information capacity is given as follows:

Definition 3 (Information Capacity): The information capacity of $\mathcal{N}$ is the maximum sum amount of the effective data that DPC can provide to the users per unit time, i.e.,

$$C_{in} = \frac{\max_{p\in P}\sum_{om_j\in OM} rd_j(p)\cdot(1 - ds_{cl_j(p)})}{T}, \tag{4}$$

where P denotes the set of all the feasible mission plans, which is determined by the given RSSN and mission set OM. $rd_j(p)$ denotes the amount of data of om_j that can be reconstructed by the DPC under mission plan p, and $cl_j(p)$ denotes the compression level chosen by mission om_j under mission plan p. □

III. ANALYTICAL FRAMEWORK OF RSSNs

In this section, we propose a graphical model which characterizes the cooperative and interactive relationships among multiple resources (including observation, computational, storage and transmission resources) during the service process of RSSNs. Then, the problem of solving the information capacity of RSSNs can be formulated into the multi-commodity flow problem under the resource conflict constraint in the graphical model.

[3]Note that although this paper only considers lossy compression, the analysis can be easily extended to incorporate lossless image compression. This is can be realized by just regarding the lossless image compression as a special case of lossy image compression with zero information loss.

A. MICROSCOPIC TIME-EXPANDED GRAPH

It is challenging to develop analytical frameworks of RSSNs due to the dynamic characters and the intertwined effect of the heterogeneous resources (e.g., observation, computational, storage and communication resources) on the information traversing process. Although the time-space graph models (e.g., time expanded graph (TEG) [27] and its extended visions [28], [29]) can be employed to model the dynamic and intertwined properties of resources, the effect of computational resource is still not taken into account. An intuitive way to tackle this problem is to modify the above graph models: when the compression condition is satisfied, reduce the value of flows after they passing by the vertices representing satellites with onboard computational resource. Nevertheless, this method breaks the flow conservation condition of the graph model, which would lead to that the classical network flow theory fails to be employed during the analysis of information capacity. Therefore, a more sophisticated graph model which not only incorporates the the effect of computational resource, but also retains the analytical characteristics of the traditional time-expanded graph is required. To this end, we further extend traditional time-expanded graph, wherein the main modifications is given as follows:

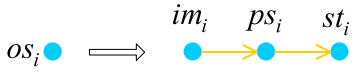

(a) Modular decomposition of a remote sensing satellite

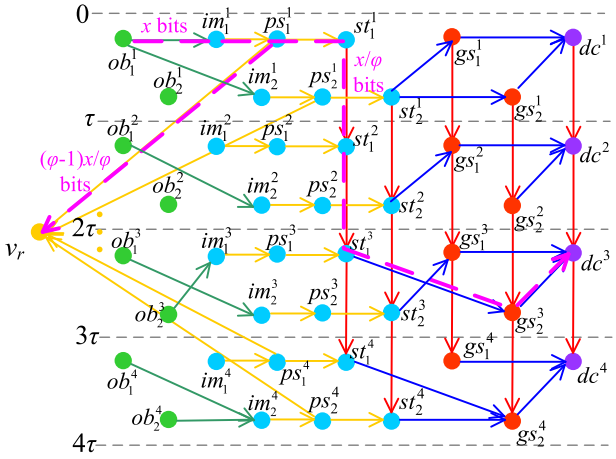

(b) Microscopic time-expanded graph

FIGURE 3. The design principle of microscopic time-expanded graph of RSSNs.

- To model the onboard compression process, we represent remote sensing satellites in a more microscopic way. To be specific, each remote sensing satellite is decomposed into three parts (as shown in Fig. 3(a)): imager, compression unit and storage-transmitter part, and each part is represented by a vertex in the graphical model.
- To guarantee the flow conservation condition, we add a virtual vertex (i.e., v_r in Fig. 3(b)) into the graph model, which connects to the vertices representing compression unit by virtual arcs. With the aid of these virtual vertex and virtual arcs, the data compression process can be modeled by a flow splitting process.

Since this extended graph model represents satellite nodes from a more microscopic point of view compared to the traditional time expanded graph, we refer it to as *microscopic time-expanded graph* (MTEG). Fig. 3(b) illustrates the MTEG of the example RSSN in Fig. 1. The MTEG of $\mathcal{N}$, denoted by $G_K(\mathcal{V}, \mathcal{A})$, is a directed graph composed of K layers. To construct the MTEG, we first divide the planning horizon $[0, T)$ into K slots, each with duration τ. Then, a snapshot is extracted from each slot to form the corresponding layer in MTEG, which represents the topology during the slot. Note that although used to model dynamic networks, MTEG are static graphs, i.e., all the arcs therein are static. In other words, with MTEG, RSSN with consecutive topology evolution can be approximated into a network of which the topology is static during each slot and only changes at slot transitions.

There are two kinds of vertices in G_K: ordinary vertices and virtual vertices, i.e, $\mathcal{V} = \mathcal{V}_o \bigcup \mathcal{V}_v$. The ordinary vertices correspond to the temporal replicas of the observation targets, imagers, compression units, storage-transmitter parts, ground stations and DPC in $\mathcal{N}$, i.e.,

$$\mathcal{V}_o = V_{ob} \bigcup V_{im} \bigcup V_{ps} \bigcup V_{st} \bigcup V_{gs} \bigcup V_{dc}, \tag{5}$$

where $V_{ob} = \{ob_i^k | 1 \le i \le |OB|, 1 \le k \le K\}$, $V_{im} = \{im_i^k | 1 \le i \le |OS|, 1 \le k \le K\}$, $V_{ps} = \{ps_i^k | 1 \le i \le |OS|, 1 \le k \le K\}$, $V_{st} = \{st_i^k | 1 \le i \le |OS|, 1 \le k \le K\}$, $V_{gs} = \{1 \le i \le |GS|, 1 \le k \le K\}$, $V_{dc} = \{dc^k | 1 \le k \le K\}$. The virtual vertices v_r is a virtual sink of the redundant information which is reduced by compression.

There are four kinds of arcs in G_K: observation arcs, link arcs, storage arcs and process arcs (represented by the green, blue, red and yellow lines in Fig. 3(b), respectively). The observation arcs model the opportunities for remote sensing satellites to acquire mission data from observation targets, i.e.,

$$A_{ob} = \{(ob_i^k, im_j^k) | \; ob_i \textit{ is in the coverage of } os_j \textit{ in the } k\textit{th slot}\}. \tag{6}$$

The capacity of observation arc $(ob_i^k, im_j^k) \in A_{ob}$, is the maximum amount of data can be acquired by remote sensing satellite os_j from observation target ob_i in the kth slot, i.e.,

$$C(ob_i^k, im_j^k) = r_{im} \cdot \tau, \tag{7}$$

where r_{im} is the data acquisition rate of remote sensing satellites. The link arcs represent the communication opportunities between remote sensing satellites and ground stations and the

links from ground stations to DPC, i.e.,

$$A_l = A_{og} \bigcup A_{gd}, \tag{8}$$

where

$$A_{og} = \{(st_i^k, gs_j^k) | os_i \textit{ locates in the coverage of } gs_j \textit{ in the } k\textit{th slot}, os_i^k \in V_{os}, gs_j^k \in V_{gs}\}, \tag{9}$$

and

$$A_{gd} = \{(gs_i^k, dc^k) | gs_i^k \in V_{gs}, dc^k \in V_{dc}\}. \tag{10}$$

The capacity of link arc $(st_i^k, gs_j^k) \in A_{og}$ is the maximum amount of data that can be transmitted by link (st_i, gs_j) in kth slot, i.e.,

$$C(st_i^k, gs_j^k) = \int_{(k-1)\tau}^{k\tau} r_{ij}(t)dt, \tag{11}$$

where $r_{ij}(t)$ is the data rate of link (st_i, gs_j). In addition, since ground stations and DPC are connected by high speed wired links, we set the capacity of arc $(gs_i^k, dc^k) \in A_{gd}$ to be infinity. The storage arcs model the storage capability of satellites, ground stations, and DPC. The storage arc set is defined as

$$A_s = \{(v_i^k, v_i^{k+1}) | v_i^k \in V_{st} \bigcup V_{gs} \bigcup V_{dc}, 1 \le k \le K-1\}. \tag{12}$$

The capacity of data storage arc (v_i^k, v_i^{k+1}), is the storage capacity of v_i, i.e.,

$$C(v_i^k, v_i^{k+1}) = sg(v_i), \tag{13}$$

where $sg(v_i)$ is the storage capacity of v_i. In addition, as ground stations and DPC are always equipped with mass storage, the storage capacity of them are assumed to be infinity.

The processing arcs represent the compress capability of the onboard image compress unit. According to the relationship with the compression vertices (i.e., ps_i^k in MTEG), there are three kind of processing arcs. The set of processing arcs is denoted by

$$A_p = A_{ip} \bigcup A_{pt} \bigcup A_{pv}, \tag{14}$$

where arcs in $A_{ip} = \{(im_i^k, ps_i^k) | 1 \le i \le |OS|, 1 \le k \le K\}$ models the connections for raw image data passing from the onboard imager to compression unit. The capacity of process arc $(im_i^k, ps_i^k) \in A_{ip}$ is set to be the maximum amount of raw image data that can be processed by the compression unit in a slot, i.e.,

$$C(im_i^k, ps_i^k) = R_p \cdot \tau, \tag{15}$$

where R_p is the processing rate of the compression unit. Arcs in $A_{pt} = \{(ps_i^k, st_i^k) | 1 \le i \le |OS|, 1 \le k \le K\}$ model the process that compressed data flow to the storage and transceiver parts from the onboard compression units. Arcs in $A_{pv} = \{(ps_i^k, v_r) | 1 \le i \le |OS|, 1 \le k \le K\}$ represent the virtual process that redundant information reduced by compression unit moving to the virtual vertex. The capacity of the processing arcs in $A_{pt} \bigcup A_{pv}$ are set to be infinite.

Through the compression vertices, virtual vertex and processing arcs, the MTEG can model the image compressing process by a flow splitting process. That is the flow from the imager vertices splits into two parts after passing by a compression vertex. The first part passes through the arcs in A_{pt}, which represents the effective data retained by compression process. The second part goes to the virtual vertex through the arcs in A_{pv}, which represents the redundant information reduced by compression process. By this way, the MTEG can not only model the the effect of computational resource, but also keeps the flow conservation condition of the network flow theory.

Thus, the MTEG can model the intertwined effect of the observation, computational, storage and communication resources on the mission complete processes of RSSNs. More specifically, the flows in the MTEG represent mission complete processes (i.e., how the observation, computational, storage and communication resource are scheduled to complete the mission) in $\mathcal{N}$. Take the flow f in Fig. 3(b) as an example, it represents that the remote sensing satellite os_1 acquires x bits raw image data from observation target ob_2 by imager im_1, and compresses the raw image under the ith level during $[0, \tau)$. After compression, $\frac{\varphi_i - 1}{\varphi_i} x$ bits are reduced. Then, the remaining x/φ_i bits data are stored in os_1 in $[\tau, 2\tau)$, and finally delivered to dc via gs_1 in $[2\tau, 3\tau)$. Therefore, the mission scheduling problem in $\mathcal{N}$ can be formulated into the multi-commodity flow problem in MTEG.

B. PROBLEM FORMULATION

As we can observe from the definition, the information capacity of RSSNs can be obtained by solving the mission plan which maximize the amount effective data outputted by the DPC. Based on the correspondence between mission complete process and the flows of METG, we can formulate the problem into a multi-community flows problem. More specifically, we firstly represent the mission execution process (i.e., information acquisition, processing, storage and transmission process) for each mission as the flows in the MTEG. For each mission om_n, to guarantee the execution process satisfy the tolerable delay requirement dy_n, the corresponding flows should pass by no more than $\lceil dy_n/\tau \rceil$ layers of MTEG. Therefore, the set of alternative executing processes of mission om_n are modeled by the set of flows

$$F_n = \{f | ob_n^k \to \{vr, dc^l\} | 0 \le \text{l-k} \le \lceil dy_n/\tau \rceil - 1\} \tag{16}$$

where $ob_n^k \to \{vr, dc^l\}$ denotes the flow originated from ob_n^k and destined to vr and dc^l in MTEG. Note that flow $ob_n^k \to \{vr, dc^l\}$ has two destination vertex, we refer v_r as virtual destination and $dc^{\lfloor te_n/\tau \rfloor}$ as original destination. Let $\mathcal{F} = \bigcup_{1 \le n \le |OM|} F_n$ denote the set of flows representing the alternative mission executing processes of all the missions.

We introduce a set of boolean vectors $\boldsymbol{y_n} = (y_n^1, y_n^2, \ldots y_n^Q)$ to indicate the compression level used by mission om_n. More specifically, if the ith compression level is employed

by mission om_n, then $y_n^i = 1$; otherwise, $y_n^i = 0$. The compression ratio selected by om_n can be expressed as $\boldsymbol{y_n}\boldsymbol{\Psi}^T$, where $\Psi = (\varphi_1, \varphi_2, \ldots, \varphi_Q)$. Let $x(f)$ denote the value of flow f. The objective is to maximize the sum effective data volume can be provided by DPC per unit time, which is expressed as

$$\frac{1}{T}\max \sum_{1\le n\le |OM|}\sum_{f\in F_n} \boldsymbol{y_n}\cdot(\boldsymbol{1}-\boldsymbol{DS})^{\boldsymbol{T}}\cdot x(f), \tag{17}$$

where $\boldsymbol{DS} = (ds_1, ds_2, \ldots ds_m)$. Let $x(v_i^k, v_j^k, f_n) > 0$ denote the amount of flow f_n on arc (v_i^k, v_j^k). Hereinafter, we introduce the constraints on the flows in $\mathcal{F}$.

Conservation Condition of Flows: As we have discussed in the previous subsection, with the introduction of virtual vertex into MTEG, the flows corresponding to mission execution process satisfy the flow conversation condition, i.e.,

$$\sum_{(v_j^l, v_i^k)\in\mathcal{A}} x(v_j^l, v_i^k, f) - \sum_{(v_i^k, v_j^l)\in\mathcal{A}} x(v_i^k, v_j^l, f) = \begin{cases} -x(f), & v_i^k = s(f) \\ 0, & v_i^k \ne s(f), d(f), v_r \\ \boldsymbol{y_n}\boldsymbol{\Lambda}^T\cdot x(f), & v_i^k = d(f) \\ (1-\boldsymbol{y_n}\boldsymbol{\Lambda}^T)\cdot x(f), & v_i^k = v_r \end{cases} \quad \forall f\in F_n,\quad 1\le n\le |OM|,\ \forall v_i^k\in\mathcal{V}_o \tag{18}$$

where $\boldsymbol{\Lambda} = (\varphi_1^{-1}, \varphi_2^{-1}, \ldots, \varphi_Q^{-1})$, and $s(f)$ and $d(f)$ denote the source and original destination vertex of flow f, respectively. The flow conversation constraint restricts that through the compression process, $1-\boldsymbol{y_n}\Lambda^T$ of the raw image data are reduced, only $\boldsymbol{y_n}\Lambda^T$ of the raw image data are required to be delivered to the DPC.

Capacity Constraints:

$$\sum_{f\in\mathcal{F}} x(v_i^k, v_j^l, f) \le C(v_i^k, v_j^l), \quad \forall (v_i^k, v_j^l)\in\mathcal{A} \tag{19}$$

The capacity constraint models the effects of the capacity of observation, processing, transmission and storage resources on the mission execution process.

Resource Conflict Constraints: There exist conflicts among the schedules of the same resource (or different resources), on account of the limited service capability of antenna/imager and the restriction of satellite platform attitude. For example, because of using single access antenna, a remote sensing satellite can only communicate with only one ground station at one slot, even if there are multiple ground stations in its coverage range. In order to model this kind of conflicts, we introduce a set of boolean variables $\delta(st_i^k, gs_j^k)$, whose value is 1 if link (st_i, gs_j) is active at the kth slot and 0 otherwise. Then, the conflicts of communication resource can be formulated as

$$\sum_{(st_i^k, gs_j^k)\in A_{og}} \delta(st_i^k, gs_j^k) \le 1, \quad \forall st_i^k\in V_{st}, \tag{20}$$

and

$$\sum_{(st_i^k, gs_j^k)\in A_{og}} \delta(st_i^k, gs_j^k) \le 1, \quad \forall gs_j^k\in V_{gs}. \tag{21}$$

Similarly, to model the conflicts among observation resource, we introduce a set of boolean variables $\delta(ob_i^k, im_j^k)$, whose value is 1 if imager im_j points at ob_i at the kth slot, and 0 otherwise. Then, we have

$$\sum_{(ob_i^k, im_j^k)\in A_{ob}} \delta(ob_i^k, im_j^k) \le 1, \quad \forall ob_i^k\in V_{ob}. \tag{22}$$

Moreover, there also exist conflicts between the schedule of communication and observation resource, when they require different platform attitude of the same remote sensing satellite. Therefore, we have

$$\delta(ob_i^k, im_j^k) + \sum_{(st_j^k, gs_l^k)\in\xi_L(ob_i^k, im_j^k)} \delta(st_j^k, gs_l^k) \le 1, \quad \forall (ob_i^k, im_j^k)\in A_{ob}, \tag{23}$$

and

$$\delta(st_i^k, gs_j^k) + \sum_{(ob_l^k, im_i^k)\in\xi_O(st_i^k, gs_j^k)} \delta(ob_l^k, im_i^k) \le 1, \quad \forall (st_i^k, gs_j^k)\in A_{og}, \tag{24}$$

where $\xi_L(ob_i^k, im_j^k)$ denotes the set of communication resources conflict with (ob_i^k, im_j^k), and $\xi_O(st_i^k, gs_j^k)$ denotes the set of observation resources conflict with (st_i^k, gs_j^k). Sets $\xi_L(ob_i^k, im_j^k)$ and $\xi_O(st_i^k, gs_j^k)$ are obtained by computing the attitude required by the scheduling of observation/transmission resource with the orbit of satellites and the location of targets/ground stations. Since no data are transmitted by non-active links, in METG flows only pass the link arcs which represent active links in corresponding time slots, i.e.,

$$\sum_{f\in\mathcal{F}} x(st_i^k, gs_j^k, f) \le \delta(st_i^k, gs_j^k) C(st_i^k, gs_j^k), \quad \forall (st_i^k, gs_j^k)\in A_{og}. \tag{25}$$

Similarly, for the observation arcs we have

$$\sum_{f\in\mathcal{F}} x(ob_i^k, im_j^k, f) \le \delta(ob_i^k, im_j^k) C(ob_i^k, im_j^k), \quad \forall (ob_i^k, im_j^k)\in A_{ob}. \tag{26}$$

Compression Constraints: For each mission om_n, only one compression level can be selected, i.e.,

$$\sum_{1\le i\le Q} y_n^i = 1, \quad \forall 1\le n\le |OM|. \tag{27}$$

To guarantee the requirement of image quality, the selected compression ratio of om_n should satisfy

$$\boldsymbol{y_n}\Psi^T \le cr_n, \quad \forall 1\le n\le |OM|. \tag{28}$$

After being acquired, the raw images of mission om_n are compressed at the compression unit with ratio $\boldsymbol{y_n}\Psi^T$. In other words, $f \in F_n$ should satisfied

$$x(im_m^{ks(f)}, ps_m^{ks(f)}, f) = \boldsymbol{y_n}\Psi^T x(ps_m^{ks(f)}, st_m^{ks(f)}, f) \quad \forall f \in F_n, \quad 1 \le n \le |OM|, \ 1 \le m \le |OS|, \quad (29)$$

where $ks(f)$ is the layer index of $s(f)$ in the MTEG.

Above all, considering all the constraints and the objective previously described, the problem of maximizing sum effective data volume obtained by DPC per unit time can be written as:

$$\mathbf{P1}: \frac{1}{T} \max \sum_{1\le n\le |OM|} \sum_{f\in F_n} (\mathbf{1} - \boldsymbol{DS})\boldsymbol{y_n^T} \cdot x(f)$$
$$s.t.\ constraints\ in\ Eq.\ (18) - Eq.\ (29)$$

In P1, $x(f)$ and $x(v_i^k, v_j^k, f)$ are continuous variables, and y_n^i and $\delta(st_i^k, gs_j^k)$ are integer variables. Besides, the constraints in Eq. (18) and Eq. (29) is non-linear. Therefore, P1 is an MINLP (mixed integer non-linear programming) problem [30], which is NP-hard in general [31].

It should be noted that although the RSSN model considered in this work is relatively simple, which only includes remote sensing satellites, ground stations and data processing center, the MTEG and the analytical framework based it are convenient to be extended to handle more complicated networks. For example, by adding vertices representing communication satellites (or data relay satellites) and drawing arcs for these vertices according to visible relationship, the MTEG can be extended to incorporate communication satellite network (or data relay system).

IV. GRAPH-BASED PROBLEM ANALYSIS AND SOLUTION

The hardness to solve problem P1 optimally mainly comes from two folds. One is the product terms which leads to P1 nolinear, and the other is the large amount of integer variables. In this section, we firstly decompose problem P1 into two sub-problems of the MTEG graphical model, i.e., flow optimization problem and arc scheduling problem. Then, we develop algorithms to solve the two sub-problems, respectively. At last, a graph-based algorithm is proposed to calculate information capacity by solving the two subproblems iteratively.

A. PROBLEM ANALYSIS AND DECOMPOSITION

Observed from the perspective of both mission completion procedure in RSSN and the flows in MTEG, the variables of problem P1 can be divided into three parts:

- Compression level indication variables $\boldsymbol{y}$: boolean variables, which indicates the compression level selected for each mission. In MTEG, y_n^i determines the splitting ratio of mission flows.
- Mission flow variables $\boldsymbol{x}$: continuous variables. $x(f)$ represents the amount data which can be provided to users for part f of mission om_i ($f \in F_i$). $x(v_i^k, v_j^k, f_n)$ represents the amount of data handled by resource (v_i^k, v_j^k). From the perspective of METG graphical model, $x(f)$ is the value of mission flow f, and $x(v_i^k, v_j^k, f)$ represents the value of f in each arc.
- Observation and communication resource scheduling variables $\boldsymbol{\delta}$: boolean variables, which indicates the schedule of observation resource and communication resource in each slot. In MTEG, $\delta(im_i^k, st_j^k)$ and $\delta(st_i^k, gs_j^k)$ indicates their corresponding observation arcs and communication arcs are active or not, respectively.

In problem P1, the compression level indication variable $\boldsymbol{y}$ are coupled with mission flow variable $\boldsymbol{x}$ by the product term in the optimization objective and the constraints in Eq. (18) and Eq. (29). As we can observe from Eq. (18) and Eq. (29), if the value of $\boldsymbol{x}$ is fixed, the value of $\boldsymbol{y}$ is also determined. Moreover, from the perspective of MTEG graphical model, compression level indication variable $\boldsymbol{y}$ and mission flow variables $\boldsymbol{x}$ jointly determine the value of flows. In comparison, observation and communication resource scheduling variables $\boldsymbol{\delta}$ determines whether an observation arcs or communication arcs is active or not. Inspired by this observation, we decompose P1 into two subproblems in MTEG to reduce its computation complexity:

1) **Flow optimization problem (FOP)**: solve $\boldsymbol{x}$ and $\boldsymbol{y}$ by optimizing the flows (i.e., the flow splitting ratio at the computation vertex, the flow value and the value on each arc) in MTEG with given arc schedule.
2) **Arc scheduling problem (ASP)**: solve $\boldsymbol{\delta}$ by scheduling the observation arcs and communication arcs without conflict in MTEG.

With the decomposition, P1 can be solved by alternatively solving the two subproblems. Algorithms are developed to solve flow optimization problem and arc scheduling problem in the following two subsections, respectively.

B. TRANSFORMATION AND SOLUTION OF FLOW OPTIMIZATION PROBLEM

Given an arc schedule, the flow optimization problem (FOP) can be obtained by fixing the observation and communication resource scheduling variables $\boldsymbol{\delta}$ in problem P1, which can be expressed as follows.

$$\mathbf{FOP}: \frac{1}{T} \max \sum_{1\le n\le |OM|} \sum_{f\in F_n} (1 - \boldsymbol{DS})\boldsymbol{y}_n^T \cdot x(f)$$
$$s.t.\ Eq.\ (18), Eq.\ (19), Eq.\ (25) - Eq.\ (29)$$
$$\boldsymbol{\delta} = \boldsymbol{\delta}_0$$

It can be observed that the obtained problem is still an MINLP, because of the integer variables $\boldsymbol{y}$ and the product terms in the objective and constraints. Note that, the only integer variables $\boldsymbol{y}$ are resulted from the discrete selection of compression ratios. With the development of onboard image compression technology, the number of compression ratios can be supported onboard increases gradually. When the adjustment of onboard compression compression ratio

tends to be continuous, the integer variable $\boldsymbol{y}$ can be approximated by continuous variable. Therefore, to solve the flow optimization problem with high speed and low complexity, we first relax the integer compression level indication variables. In this case, y_n^i can be considered as the selection weight of compression ratios, and the selected compression ratio can be approximated by $\boldsymbol{y}_n\boldsymbol{\Psi}^T$. Thus, FOP can be transferred into an LP (Linear Programming) problem through replacing the product term. Specifically, we consider the transformation

$$\hat{x}_n^i(f) = x(f) \cdot y_n^i. \tag{30}$$

Based on this transformation, the objective can be reformulated into

$$\frac{1}{T} \max \sum_{1 \le n \le |OM|} \sum_{f \in F_n} \hat{\boldsymbol{x}}_n(f) \cdot (1 - \boldsymbol{DS})^T,$$

where vector $\hat{\boldsymbol{x}}_n(f) = (\hat{x}_n^1(f), \hat{x}_n^2(f), \ldots, \hat{x}_n^Q(f))$. Combining Eq. (30) and Eq. (27), we have the following transformation

$$x(f) = x(f) \cdot \sum_{1 \le i \le Q} y_n^i = \sum_{1 \le i \le Q} \hat{x}_n^i(f) \tag{31}$$

By substitute Eq. (30) and Eq. (31) into Eq. (18), the flow conservation constraint can be reformulated as

$$\sum_{(v_j^l, v_i^k) \in \mathcal{A}} x(v_j^l, v_i^k, f) - \sum_{(v_i^k, v_j^l) \in \mathcal{A}} x(v_i^k, v_j^l, f)$$
$$= \begin{cases} -\sum_{1 \le i \le Q} \hat{x}_n^i(f), & v_i^k = s(f) \\ 0, & v_i^k \ne s(f), d(f), v_r \\ \hat{\boldsymbol{x}}_n(f)\boldsymbol{\Lambda}^T, & v_i^k = d(f) \\ \sum_{1 \le i \le Q} \hat{x}_n^i(f) - \hat{\boldsymbol{x}}_n(f)\boldsymbol{\Lambda}^T, & v_i^k = v_r \end{cases}$$
$$\forall f \in F_n, \quad 1 \le n \le |OM|, \ \forall v_i^k \in \mathcal{V}_o \tag{32}$$

Similarly, the constraint in Eq.(29) can be reformulated as

$$\hat{\boldsymbol{x}}_n(f)\boldsymbol{\Lambda}^T = x(ps_m^{ks(f)}, st_m^{ks(f)}, f)$$
$$\forall f \in F_n, 1 \le n \le |OM|, 1 \le m \le |OS| \tag{33}$$

In summary, by means of the transformation in Eq. (30) and Eq. (31), we can reformulate flow optimization problem as

$$\textbf{FOLP}: \frac{1}{T} \max \sum_{1 \le n \le |OM|} \sum_{f \in F_n} \hat{\boldsymbol{x}}_n(f) \cdot (1 - \boldsymbol{DS})^T$$
$$s.t.\ Eq.\ (32), Eq.\ (19), Eq.\ (25) - Eq.\ (28), Eq.\ (33)$$
$$\boldsymbol{\delta} = \boldsymbol{\delta}_0$$

It can be observed that the reformulation of the flow optimization problem, referred to as FOLP, is an LP (Linear Program) problem, which can be solved with polynomial time. Based on the results $\hat{x}_n^i(f)$ of FOLP, the relaxed compression level indication variables $\tilde{\boldsymbol{y}}$ can be obtained by following expression.

$$\tilde{\boldsymbol{y}}_n = \frac{\hat{\boldsymbol{x}}_n(f)}{\sum_{1 \le i \le Q} \hat{x}_n^i(f)}, \quad \forall 1 \le n \le |OM| \tag{34}$$

Then, the compression level of each mission can be determined by rounding the sum of compression levels weighted by $\tilde{\boldsymbol{y}}$, i.e.,

$$r = round(\sum_{1 \le i \le Q} \tilde{y}_n^i \cdot i), \quad \forall 1 \le n \le |OM| \tag{35}$$

At last, we solve FOP with fixed $\boldsymbol{y}$ to obtain mission flow variables $\boldsymbol{x}$ and information capacity C_{in}. Algorithm 1 summarizes the detailed procedure of solving the flow optimization problem.

Algorithm 1 Solution of Flow Optimization Problem

```
Input: MTEG G_K(V, A), OM, δ_0.
Onput: x, y, C_in.
Construct FOLP with δ_0;
Solve FOLP;
for 1 ≤ n ≤ |OM| do
    ỹ_n = x_n(f) / Σ_{1≤i≤Q} x̂_n^i(f);
    r ← round(Σ_{1≤i≤Q} ỹ_n^i · i);
    y_n^i ← 1, i = r;
    y_n^i ← 0, ∀i ≠ r;
end for
Solve FOP with fixed y;
```

C. GRAPH-BASED SOLUTION OF ARC SCHEDULING PROBLEM

1) CONFLICT GRAPH FOR OBSERVATION AND COMMUNICATION RESOURCES

As we have discussed in Section III.B, the schedule of different observation and/or communication resources may conflict with each other due to the limited service capability of antenna/imager and the restriction of satellite platform attitude. To provide a conflict-free schedule in MTEG, we propose conflict graph, denoted by CG, to model the conflict relationship among different resources.

Fig. 4 depicts the conflict graph of the observation and communication resources shown in Fig. 3(b). Each node in conflict graph represents a possible resource schedule which corresponds to an arc in MTEG. For example, node $nd(ob_1^1, im_1^1)$ in Fig. 4 represents the schedule that the observation resource of satellite os_1 (i.e., im_1) observes ob_1 in the 1st slot, which corresponds to arc (ob_1^1, im_1^1) in Fig. 3(b). The edges in conflict graph represent the conflicts between the resource schedules. In other words, if there two resource schedules conflicts with each other, there exist an edge between the two nodes corresponding to them in CG. According to the source of conflicts, the edges of conflict graph can be divided into two categories:

- Resource service restriction edges: represent the conflicts caused by the limitation on the number services supported by observation and communication resources at the same time. For example, edge $nd(st_1^1, gs_1^1) \leftrightarrow nd(st_1^1, gs_2^1)$ represents the conflict that in the 1st slot

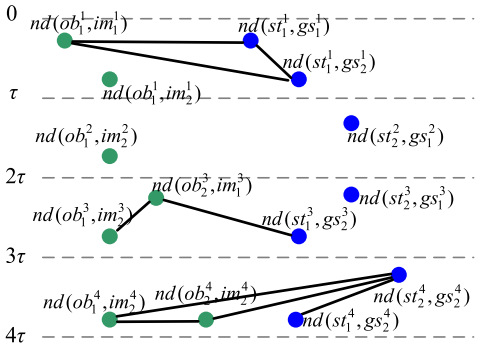

FIGURE 4. Conflict Graph for observation and communication resources.

satellite os_1 can only communicate with one ground station of gs_1 and gs_2.

- Platform attitude restriction edges: represent the conflicts resulted in the different requirement of platform attitude to a satellite. For example, edge $nd(ob_2^3, im_1^3) \leftrightarrow nd(st_1^3, gs_2^3)$ represents the conflicts that in the 3rd slot satellite os_1 can either observe ob_2 or communicate with ground station gs_2, due to the different platform attitude requirement of os_1.

Similar to MTEG, the conflict graph is a layered graph. Moreover, the layers of conflict graph are independent with each other, because the edges only connect nodes in the same layer. The resource schedules contained in an independent set[4] of conflict graph are conflict-free, since there exists no edge between the nodes of an independent set in CG. Therefore, through sequentially finding independent sets for each layer of the conflict graph, an conflict-free schedule of observation and communication arcs can be obtained.

2) INITIALIZATION OF OBSERVATION AND COMMUNICATION ARC SCHEDULE

An IASC (Initial Arc Schedule Construction) algorithm is proposed to construct a conflict-free schedule of observation and communication arcs through conflict graph at the beginning of alternatively solving FOP and ASP problem. In order to accelerate the convergence speed, an effective initial arc schedule should be constructed to obtain a good solution for the following flow optimization problem. To achieve this goal, we strike a balance between the scheduled observation and communication resources to avoid wasting the scheduled resources. To this end, the main idea of IASC algorithm is to set weight for the nodes according to the ratio of the capacity scheduled observation and communication arcs, and then find the maximum weight independent set in the conflict graph layer by layer.

Algorithm 2 details the complete procedure of IOCAS algorithm, which consists of two stages. In the first stage, the compression level r is initialized as follows.

$$r = \arg \max_{1 \le i \le Q} \{(1 - ds_i)\varphi_i\} \tag{36}$$

Then, we search for the observation and communication resources which have opportunities to complete a mission, and set the weights of them in the conflict graph to 1.

In the second stage, the arc schedule is solved through conflict graph layer by layer. For each layer, we firstly set the weight of the nodes corresponding to observation arcs to ρ, which is expressed as

$$\rho = \frac{c_c \cdot \varphi_r}{c_o}, \tag{37}$$

wherein c_o and c_c are the sum capacity of the scheduled observation and communication arcs, respectively. Weight ρ is designed to strike a balance between the scheduled observation and communication resources so that achieve a high resource utilization. For example, when $c_o > c_c \cdot \varphi_r$, the capacity of scheduled observation resources is larger than amount of effective data the scheduled communication resources can transmit even with the help of data compression. This means part of observation resources in the preceding layers cannot be fully utilized. In this case, weight of observation arcs are set to $\rho < 1$ to reduce the ratio of scheduled observation resources in the succeeding layers. Secondly, we solve the maximum independent set[5] of current layer. After all the layers have been traversed, we obtain the independent set of conflict graph IS by combining the independent sets of each layer and thus obtain the observation and communication resource scheduling variables.

3) UTILIZATION ORIENTED ARC SCHEDULING

A UOASU (Utilization Oriented Arc Schedule Update) algorithm is proposed to improve the arc schedule based on the solution of flow optimization problem. As shown in Algorithm 3, we firstly search the set of scheduled resources with low utilization, denoted by A_{LU}. Then, for each arc in A_{LU} (without loss of generality, denoted by (v_i^k, v_j^k)), the weight of nodes in the same layer of CG are reset to improve the opportunities of other resources to be scheduled. More specifically, for the node corresponding to arc in A_{LU}, its weight is reset to its utilization, i.e., $\frac{x_0(v_i^k, v_j^k)}{C(v_i^k, v_j^k)}$. For the other nodes, the new weight is expressed as

$$w(v_m^k, v_n^k) = \alpha \frac{x_0(v_i^k, v_j^k)}{C(v_i^k, v_j^k)} + \left(1 - \alpha \cdot \delta_0(v_m^k, v_n^k)\right) \varpi,$$
$$\forall (v_m^k, v_n^k) \in A_{ob} \bigcup A_{og}, \quad m \neq i, \ n \neq j \tag{38}$$

wherein $0 < \alpha < 1$ and $\varpi \sim U(0, 1)$ is a uniformly distributed random variable in (0,1). After the weights of all

[4]The independent set in graph G is a set of nodes such that there is no two nodes are adjacent in G [32].

[5]Note that the size of each layer in conflict graph is small because of the limited number of satellites in RSSNs. Therefore, in spite of the maximum weight independent set is NP-complete [33], we can solve it within limited time through either enumerative methods (e.g. branch-and-bound algorithms [34]) or approximation heuristic algorithm [35].

Algorithm 2 Initial Arc Schedule Construction

Input: conflict graph CG, OM.
Onput: $\boldsymbol{\delta}$.
Initialize: $\rho = 1$, $\boldsymbol{w} = \mathbf{0}$, $\boldsymbol{\delta} = \mathbf{0}$, $c_o = 0$, $c_c = 0$.
$r \leftarrow \arg\max_{1 \le i \le Q} \{(1 - ds_i)\varphi_i\}$;
for $1 \le n \le |OM|$ **do**
  for each $(ob_n^k, im_i^k) \in \mathcal{A}$ **do**
    if $\exists (st_i^l, gs_j^l) \in \mathcal{A}$ and $l - k \le \frac{dy_n}{\tau}$ **then**
      $w(ob_n^k, im_i^k) \leftarrow 1$;
      $w(st_i^l, gs_j^l) \leftarrow 1, \forall (st_i^l, gs_j^l) \in \mathcal{A}$ and $l - k \le \frac{dy_n}{\tau}$;
    end if
  end for
end for
for $1 \le k \le K$ **do**
  $w(ob_j^k, im_i^k) \leftarrow w(ob_j^k, im_i^k) \cdot \rho, \forall (ob_j^k, im_i^k) \in \mathcal{A}$;
  find maximum weight independent set of CG_k;
  $c_o \leftarrow c_o + \sum_{(ob_i^k, im_j^k) \in In_k} C(ob_i^k, im_j^k)$;
  $c_c \leftarrow c_c + \sum_{(st_i^k, gs_j^k) \in In_k} C(st_i^k, gs_j^k)$;
  $\rho \leftarrow \frac{c_c \cdot \varphi_r}{c_o}$;
end for
$IS = \cup_{1 \le k \le K} IS_k$;
$\delta(v_i^k, v_j^k) \leftarrow 1, \forall (v_i^k, v_j^k) \in IS$

Algorithm 3 Utilization Oriented Arc Schedule Update

Input: CG, OM, $\boldsymbol{x}_0$, $\boldsymbol{\delta}_0$.
Onput: $\boldsymbol{\delta}$.
Initialize: $\boldsymbol{w} = \mathbf{0}$, $\boldsymbol{\delta} = \boldsymbol{\delta}_0$.
$A_{LU} \leftarrow \{(v_i^k, v_j^k) | (v_i^k, v_j^k) \in A_{ob} \bigcup A_{og}, \frac{x_0(v_i^k, v_j^k)}{C(v_i^k, v_j^k)} < U_T\}$
for each $(v_i^k, v_j^k) \in A_{LU}$ **do**
  $w(v_i^k, v_j^k) \leftarrow \frac{x_0(v_i^k, v_j^k)}{C(v_i^k, v_j^k)}$
  $w(v_m^k, v_n^k) \leftarrow \frac{1}{2}\delta_0(v_m^k, v_n^k) + \left(1 - \frac{1}{2}\delta_0(v_m^k, v_n^k)\right)\varpi$, $\forall (v_m^k, v_n^k) \in A_{ob} \bigcup A_{og}, m \ne i, n \ne j$;
  find the maximum weighted independent set of the k-th layer of CG, and then update corresponding arc scheduling variables in $\boldsymbol{\delta}$;
end for

nodes in the k-th layer being reset, we find the maximum weighted independent set of the k-th layer of CG, and then update corresponding arc scheduling variables in $\boldsymbol{\delta}$.

D. GRAPH-BASED INFORMATION CAPACITY SOLVING ALGORITHM

Based on the decomposition of P1 and the algorithms to its subproblems, a graph-based algorithm is proposed to solving the information capacity. The outline of GBICS (graph-based information capacity solving) algorithm is illustrated in Algorithm 4. It firstly initialize a conflict-free schedule of observation and communication arcs by IASC algorithm. Then, we can obtain a initialized solution of P1 through SFOP

Algorithm 4 Graph-Based Information Capacity Solving

1: **Input:** MTEG $G_K(\mathcal{V}, \mathcal{A})$, Mission demand OM.
2: **Onput:** Information Capacity C_{in}.
3: **Initialize:** $t = 1$.
4: $\boldsymbol{\delta}_0 \leftarrow IASC\ (G_K(\mathcal{V}, \mathcal{A}), OM)$.
5: $(C_{in}^0, \boldsymbol{x}_0, \boldsymbol{y}_0) \leftarrow SFOP\ (G_K(\mathcal{V}, \mathcal{A}), OM, \boldsymbol{\delta}_0)$
6: **while** $t < M_T$ **do**
7: $\boldsymbol{\delta} \leftarrow UOASU\ (G_K(\mathcal{V}, \mathcal{A}), OM, \boldsymbol{x}_0, \boldsymbol{\delta}_0)$;
8: $(C_{in}, \boldsymbol{x}, \boldsymbol{y}) \leftarrow SFOP\ (G_K(\mathcal{V}, \mathcal{A}), OM, \boldsymbol{\delta})$;
9: **if** $C_{in} > C_{in}^0$ **then**
10: $(C_{in}^0, \boldsymbol{x}_0, \boldsymbol{y}_0, \boldsymbol{\delta}_0) \leftarrow (C_{in}, \boldsymbol{x}, \boldsymbol{y}, \boldsymbol{\delta})$;
11: **else**
12: generate a random number $\varpi \sim U(0, 1)$;
13: **if** $e^{\frac{C_{in} - C_{in}^0}{\beta^t \cdot M_R}} > \varpi$ **then**
14: $(C_{in}^0, \boldsymbol{x}_0, \boldsymbol{y}_0, \boldsymbol{\delta}_0) \leftarrow (C_{in}, \boldsymbol{x}, \boldsymbol{y}, \boldsymbol{\delta})$;
15: **end if**
16: **end if**
17: $t \leftarrow t + 1$;
18: **end while**

algorithm. Afterwards, the flow optimization problem and arc scheduling problem are solved iteratively by UOSAU algorithm and SFOP algorithm, respectively. More specifically, in each iteration, if the new solution is better than the current one, it is accepted. Otherwise, the new solution is accepted with probability $e^{\frac{C_{in} - C_{in}^0}{\beta^t \cdot M_R}}$ as illustrated in line 12-14 of Algorithm 4, wherein $0 < \beta < 1$ and $M_R \gg 1$. It should be noted that the probability decreases with the difference between the new solution and current one $C_{in} - C_{in}^0$ and iteration number t. When t is small, the acceptance probability is large to avoid being stuck in a local optimum at early iterations. When t get large, the acceptance probability become small to accelerate convergence.

V. SIMULATIONS

In this section, simulation results are presented to validate our analysis and investigate information capacity of RSSNs. We conduct a baseline scenario which consists of 20 remote sensing satellites, 6 ground stations and one data processing center. The remote sensing satellites locate in four sun-synchronous orbits at a height of 619.6km and with inclination 97.86°. The pitching and rolling angle of remote sensing satellites can vary among range $[-45°, 45°]$ and $[-30°, 30°]$, respectively. Each remote sensing satellite is equipped with an imager, a image compressing unit, a transceiver and a storage. The swath and resolution of the imager is 60km and 2m, respectively. The data quantization of the raw images is with 10bit. The image compressing unit can supports 4 compression ratios, which are 4:4, 4:3, 4:2, 4:1. The transmission rate of the transceiver is 50Mbps. The storage capacity is 100Gbit. The six ground stations locate at Beijing (40°N, 116°E), Sanya (18°N, 109.5°E), Kashi (39.5°N, 76°E), White Sands (34°N, 105°W), Santiago

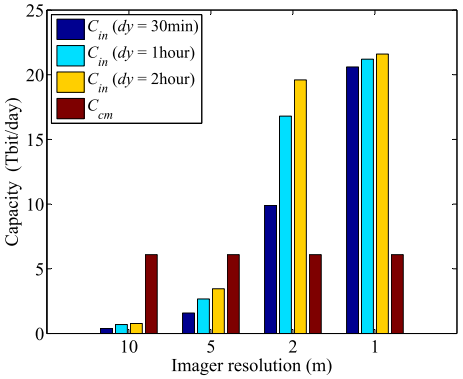

FIGURE 5. The information/communication capacity varying with observation capability.

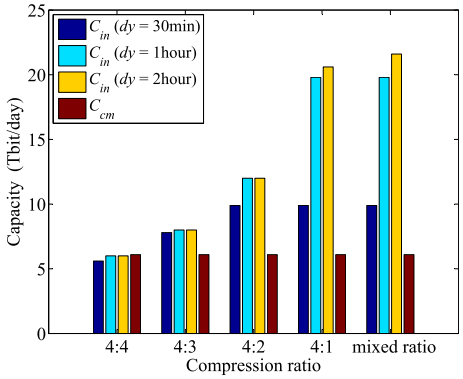

FIGURE 6. The information/communication capacity varying with computational capability.

(33.5°S, 70.5°W), and Fracati (41.5°N, 12.5°E), respectively. The antennas of ground stations are with minimum elevation angle of 10°. There are 80 missions, of which the observation targets are uniformly distributed on the earth's surface. The tolerable delay of the missions are varying from 30min to two hours. The planning horizon is from 11 Jun 2019 04:00:00 to 12 Jun 2019 04:00:00. The length of a time slot is set to 1 minute.[6]

A. INFORMATION CAPACITY WITH VARYING CAPABILITY OF DIFFERENT RESOURCES

In this subsection, we investigate the impacts of different resources on information capacity, and show the difference between information capacity and traditional communication capacity [12]. To evaluate the impact of observation resource on information capacity, we varying the resolution of the imagers from 10m to 1m and show the information capacity when tolerable delay is 0.5h, 1h and 2h in Fig. 5. As expected, the communication capacity is not varying with the capability of observation resource, because it does not take into account the information acquisition process. In comparison, the information capacity is non-decreasing with the capability of observation resource. To be specific, when the tolerable delay is small, the information capacity is near linearly increasing with the data acquisition rate. This is because due to the small tolerable delay, only the data acquired from the observation targets near ground stations have opportunities to be downloaded, which results in the underutilization of downloading links. In this case, the larger data acquisition rate is, the more data can be download. When the tolerable delay is large, the growth of information capacity become slow with the capability of observation resource until stagnation. This is because in this case the data from much more observation targets can be delivered through store-carry-forward paradigm. Therefore, when the data acquisition rate is too large, the information capacity is restricted by the capacity of other resources.

[6]In practical application, the principle of deciding the value of τ is to strike a balance between the accuracy of the model and computational complex.

Fig. 6 depicts the relationship of information (and communication) capacity with varying capability of computational resource. As can be observed, the communication capacity is not varying with the capability of computational resource, since it does not consider the information processing process. When the tolerable delay is small, the information capacity increases slowly with the compression ratio. This is because with the small tolerable delay, the transmission and storage capability is large enough for most images without compression. When the tolerable delay is large, the growth of information capacity is nearly linear with the compression ratio. In this case, the amount of acquired data is much larger than the transmission capacity. Therefore, the larger the compression ratio is, the more effective information can be downloaded.

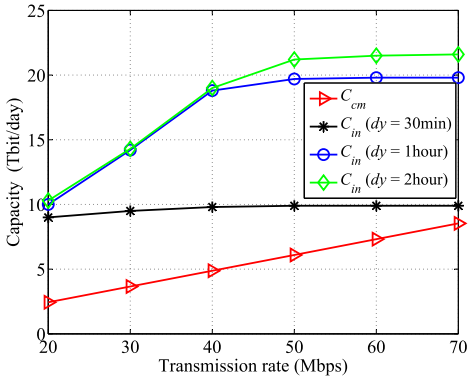

FIGURE 7. The information/communication capacity varying with communication capability.

To evaluate the impact of communication resource on network capacity, we varying the transmission rate from 20Mbps to 70Mbps and plot the communication capacity and the information capacity when tolerable delay is 0.5h, 1h and 2h in Fig. 7. As expected, the communication capacity increases linearly with the capability of communication resource. In comparison, the information capacity has near-liner growth with the capability of communication resource at first, and then tends to become nonlinear saturation, because of the

limitation of other resources. More specifically, when the tolerable delay is small, the information capacity hardly changes with the transmission rate. This is because due to the small tolerable delay, only the data acquired from the observation targets near ground stations have opportunities to be downloaded, thus the downloading capacity is always larger than the amount of acquired data. When the tolerable delay is large, the information capacity has near-liner growth with the capability of communication resource for a longer period, and then tends to saturation. This is because in this case large amount of acquired data can be delivered via store-carry-forward paradigm, thus large downloading capability is required. Therefore, the larger the transmission rate is, the more effective information can be downloaded.

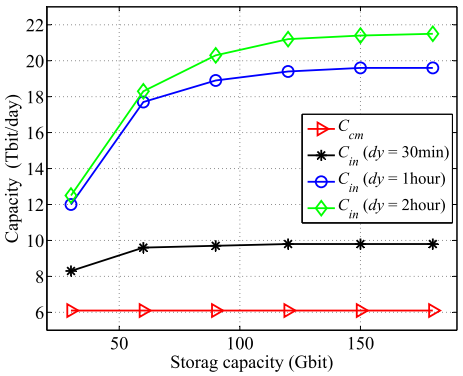

FIGURE 8. The information/communication capacity varying with storage capability.

At last, we investigate the impact of storage resource on information capacity, and show the difference between information capacity and traditional communication capacity. Fig. 8 depicts the information capacity and communication capacity when the storage capacity varies from 30Gbit to 180Gbit. As can be observed, the communication capacity is not varying with the capability of storage resource, since it does not consider the impact of storage resources. In comparison, the information capacity is non-decreasing with the capability of storage resource. To be specific, when the tolerable delay is small, the information capacity tends to become saturation after a short period of near-linear growth. This is because in this case only the data acquired from the observation targets near ground stations have opportunities to be downloaded, thus the required storage capacity is very limited. When the tolerable delay is large, the information capacity has near-liner growth with the capability of communication resource for a longer period, and then tends to saturation. This is because in this case large amount of data can be delivered via store-carry-forward paradigm, thus large amount of storage capacity is required.

B. INFORMATION CAPACITY WITH VARYING NETWORK ARCHITECTURAL PARAMETERS

In this subsection, we investigate the impacts of different network architectural parameters (e.g., the orbital parameters of the satellites and the distribution of the ground stations) on information capacity, and show the difference between information capacity and traditional communication capacity. Four new simulation scenarios are conducted by changing one parameter of the baseline scenario (referred to as S0). Note that to investigate the impact of different parameter separately, each new scenario has only one parameter different from S0. Here, for the sake of brevity, for each new scenario we only list the parameter different from the baseline scenario.

- **S1:** The altitude of remote sensing satellites is 500km.
- **S2:** The altitude of remote sensing satellites is 1000km.
- **S3:** The six ground stations locate at Beijing (40°N, 116°E), Sanya (18°N, 109.5°E), Kashi (39.5°N, 76°E), Weinan (34.5°N, 109.5°E), Xiamen (25.5°N, 118°E), Jiamusi (46.5°N, 130°E).
- **S4:** The six ground stations locate at Kiruna (68°N, 20°E), Fairbank (65°N, 148°W), Jiamusi (46.5°N, 130°E), Huanghe (79°N, 12°E), Helsinki (60°N, 25°E), Ushuaia (55°S, 68.5°W).

Hereinafter, we compare the simulation results and explore the influence of satellite altitude and development of ground stations on the network capacity.

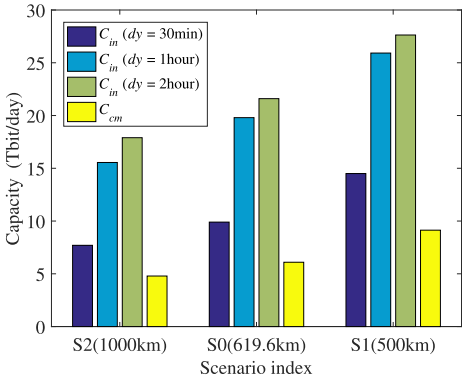

FIGURE 9. The information/communication capacity varying with different altitude of remote sensing satellites.

Fig. 9 illustrates the influence of varying altitude of remote sensing satellites on both communication and information capacity. It can be observed that both capacity increase with altitude. This is because the length of visible windows between the satellites and ground stations/observation targets increases with the altitude of remote sensing satellites. Moreover, the variation of communication capacity with altitude is more obvious than that of information capacity especially when tolerant delay is large. This is because the communication capacity increases linearly with the communication windows. In comparison, although high altitude brings more observation and transmission opportunities, the information capacity still be limited by the contention among resource scheduling and the amount of storage and computational resource, especially with large tolerant delay.

Fig. 10 illustrates the influence of different ground station deployment on both communication and information

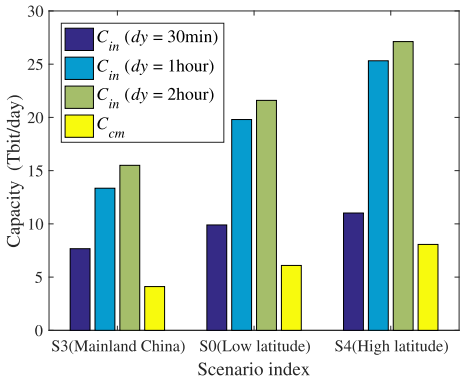

FIGURE 10. The information/communication capacity varying different ground station deployment.

capacity. In scenario S3, we deploy ground stations only on China mainland. In scenario S0, we deploy the ground stations globally and choose the locations with lower latitude. In scenario S4, we deploy the ground stations globally and choose the locations with higher latitude. As can be seen from Fig. 10, the global deployment performs better than the local deployment, and the deployment at higher latitudes performs better than the deployment at lower latitudes. This is because the global deployment can avoid the overlap of the coverage areas of the ground stations. Moreover, because the remote sensing satellites fly on near-polar orbits, the visible time for a ground station increases with the latitude of the ground station. Therefore, both global and high latitude deployment of ground stations can bring more downloading opportunities for remote sensing satellites.

VI. CONCLUSION

In this paper, we explore the information capacity of RSSNs. We first propose the formal definition of information capacity. Then, we extend traditional time-expanded graph by modeling remote sensing satellites in a microscopic level and adding virtual arcs and virtual vertex. A new graph model called microscopic time-expanded graph (MTEG) is developed, which characterizes the intertwined impact of the observation, computational, storage and transmission resources on the service process. Base on this graph model, we develop a mathematical framework to compute the information capacity. Owing to the NP-completeness of the formulated problem, we decompose it into a flow optimization problem and an arc scheduling problem of the MTEG model, and then propose a Graph-based Information Capacity Solving (GICS) algorithm to efficiently solve the problem. Finally, extensive simulation results are provided to validate the effectiveness and necessity of analysis of information capacity in RSSNs. The impacts of different kinds of resources and network architectural parameters on the information capacity are evaluated.

REFERENCES

[1] A. M. Elhady, "Remote sensing satellite system overall effectiveness analysis and modeling," in *Proc. IEEE Aerosp. Conf.*, Mar. 2014, pp. 1–10.

[2] J. N. Pelton, "Key trends in remote-sensing satellite systems and services," in *Space 2.0: Revolutionary Advances Space Industry*. Cham, Switzerland: Springer, 2019, pp. 31–45.

[3] Y. Zhu, M. Sheng, J. Li, R. Liu, Y. Wang, and K. Chi, "Traffic modeling and performance analysis for remote sensing satellite networks," in *Proc. IEEE Global Commun. Conf. (GLOBECOM)*, Dec. 2018, pp. 1–6.

[4] Y. Zheng, S. Zhao, Q. Tan, Y. Li, Y. Jiang, and N. Xin, "An analytical framework for remote sensing satellite networks based on the model predictive control with convex optimization," *Int. J. Satell. Commun. Netw.*, vol. 36, no. 3, pp. 305–314, May 2018.

[5] P. Li, M. Pan, and Y. Fang, "Capacity bounds of three-dimensional wireless ad hoc networks," *IEEE/ACM Trans. Netw.*, vol. 20, no. 4, pp. 1304–1315, Aug. 2012.

[6] N. Lu and X. S. Shen, "Scaling laws for throughput capacity and delay in wireless networks —A survey," *IEEE Commun. Surveys Tuts.*, vol. 16, no. 2, pp. 642–657, 2nd Quart., 2014.

[7] Z. Wei, H. Wu, X. Yuan, S. Huang, and Z. Feng, "Achievable capacity scaling laws of three-dimensional wireless social networks," *IEEE Trans. Veh. Technol.*, vol. 67, no. 3, pp. 2671–2685, Mar. 2018.

[8] P. Gupta and P. R. Kumar, "The capacity of wireless networks," *IEEE Trans. Inf. Theory*, vol. 46, no. 2, pp. 388–404, Mar. 2000.

[9] R. Liu, M. Sheng, K.-S. Lui, X. Wang, D. Zhou, and Y. Wang, "Capacity analysis of two-layered LEO/MEO satellite networks," in *Proc. IEEE 81st Veh. Technol. Conf. (VTC Spring)*, May 2015, pp. 1–5.

[10] R. Liu, M. Sheng, K.-S. Lui, X. Wang, D. Zhou, and Y. Wang, "Capacity of two-layered satellite networks," *Wireless Netw.*, vol. 23, no. 8, pp. 2651–2669, Nov. 2017.

[11] S. C. Spangelo, D. Boone, and J. Cutler, "Assessing the capacity of a federated ground station," in *Proc. IEEE Aerosp. Conf.*, Mar. 2010, pp. 1–9.

[12] S. C. Spangelo, J. W. Cutler, A. T. Klesh, and D. R. Boone, "Models and tools to evaluate space communication network capacity," *IEEE Trans. Aerosp. Electron. Syst.*, vol. 48, no. 3, pp. 2387–2404, Jul. 2012.

[13] L. Li, S. Li, and S. Zhao, "QoS-aware scheduling of services-oriented Internet of Things," *IEEE Trans. Ind. Informat.*, vol. 10, no. 2, pp. 1497–1505, May 2014.

[14] J. Wu, M. Dong, K. Ota, J. Li, W. Yang, and M. Wang, "Fog-computing-enabled cognitive network function virtualization for an information-centric future Internet," *IEEE Commun. Mag.*, vol. 57, no. 7, pp. 48–54, Jul. 2019.

[15] E. K. Markakis, K. Karras, A. Sideris, G. Alexiou, and E. Pallis, "Computing, caching, and communication at the edge: The cornerstone for building a versatile 5G ecosystem," *IEEE Commun. Mag.*, vol. 55, no. 11, pp. 152–157, Nov. 2017.

[16] C. Wang, C. Liang, F. R. Yu, Q. Chen, and L. Tang, "Computation offloading and resource allocation in wireless cellular networks with mobile edge computing," *IEEE Trans. Wireless Commun.*, vol. 16, no. 8, pp. 4924–4938, Aug. 2017.

[17] P. Tangpattanakul, N. Jozefowiez, and P. Lopez, "A multi-objective local search heuristic for scheduling Earth observations taken by an agile satellite," *Eur. J. Oper. Res.*, vol. 245, no. 2, pp. 542–554, Sep. 2015.

[18] J. Du, C. Jiang, J. Wang, Y. Ren, S. Yu, and Z. Han, "Resource allocation in space multiaccess systems," *IEEE Trans. Aerosp. Electron. Syst.*, vol. 53, no. 2, pp. 598–618, Apr. 2017.

[19] H. Lu, Y. Gui, X. Jiang, F. Wu, and C. W. Chen, "Compressed robust transmission for remote sensing services in space information networks," *IEEE Wireless Commun.*, vol. 26, no. 2, pp. 46–54, Apr. 2019.

[20] M. L'Abbate, P. Venditti, C. Svara, F. Bagaglini, and R. Roscigno, "From Mbps to Gbps: Evolution of payload data handling and transmission system for future earth observation missions," in *Proc. IEEE Metrology for Aerosp. (MetroAeroSpace)*, May 2014, pp. 576–581.

[21] P. Pavia, G. Spera, R. Venturini, F. Bagaglini, S. Lunardini, E. Scorzafava, and E. Miotti, "CSG satellite design and performance," in *Proc. 11th Eur. Conf. Synth. Aperture Radar*, Jun. 2016, pp. 1–4.

[22] N. R. Mat Noor and T. Vladimirova, "Investigation into lossless hyperspectral image compression for satellite remote sensing," *Int. J. Remote Sens.*, vol. 34, no. 14, pp. 5072–5104, Jul. 2013.

[23] L. N. Faria, L. M. G. Fonseca, and M. H. M. Costa, "Performance evaluation of data compression systems applied to satellite imagery," *J. Elect. Comput. Eng.*, vol. 2012, Apr. 2012, Art. no. 471857.

[24] K. Manthey, D. Krutz, and B. Juurlink, "Reconfigurable architecture for real-time image compression on-board satellites," *J. Appl. Remote Sens*, vol. 9, no. 1, Jun. 2015, Art. no. 097497.

[25] G. Yu, T. Vladimirova, and M. N. Sweeting, "Image compression systems on board satellites," *Acta Astronautica*, vol. 64, nos. 9–10, pp. 988–1005, May 2009.
[26] A. M. Eskicioglu and P. S. Fisher, "Image quality measures and their performance," *IEEE Trans. Commun.*, vol. 43, no. 12, pp. 2959–2965, Dec. 1995.
[27] L. R. Ford and D. R. Fulkerson, *Flows in Networks*. Princeton, NJ, USA: Princeton Univ. Press, 1962.
[28] R. Liu, M. Sheng, K.-S. Lui, X. Wang, Y. Wang, and D. Zhou, "An analytical framework for resource-limited small satellite networks," *IEEE Commun. Lett.*, vol. 20, no. 2, pp. 388–391, Feb. 2016.
[29] M. Sheng, Y. Wang, J. Li, R. Liu, D. Zhou, and L. He, "Toward a flexible and reconfigurable broadband satellite network: Resource management architecture and strategies," *IEEE Wireless Commun.*, vol. 24, no. 4, pp. 127–133, Aug. 2017.
[30] D. P. Bertsekas, *Nonlinear Programming*. Belmont, MA, USA: Athena Scientific, 1999.
[31] M. R. Gary and D. S. Johnson, *Computers and Intractability, A Guide To The Theory of NP-Completenes*. New York, NY, USA: W.H. Freeman and Company, 1979.
[32] J. A. Bondy and U. S. R. Murty, *Graph Theory With Applications*. London, U.K.: Macmillan, 1976.
[33] M. R. Garey and D. S. Johnson, *Computers and Intractability, A Guide To The Theory of NP-Completeness*. New York, NY, USA: W. H. Freeman, 1979.
[34] D. Warrier, W. E. Wilhelm, J. S. Warren, and I. V. Hicks, "A branch-and-price approach for the maximum weight independent set problem," *Networks*, vol. 46, no. 4, pp. 198–209, Dec. 2005.
[35] S. Sanghavi, D. Shah, and A. S. Willsky, "Message passing for maximum weight independent set," *IEEE Trans. Inf. Theory*, vol. 55, no. 11, pp. 4822–4834, Nov. 2009.

RUNZI LIU (Member, IEEE) received the B.S. degree (Hons.) in telecommunications engineering and the Ph.D. degree in communication and information systems from Xidian University, Xi'an, China, in 2011 and 2016, respectively. From 2016 to 2019, she held a postdoctoral position with the State Key Laboratory of ISN, Xidian University. In 2019, she joined the Xi'an University of Architecture and Technology, where she is currently an Associate Professor. She has been a Floating Researcher with the Science and Technology on Communication Networks Laboratory, 54th Research Institute of CETC, since 2019. Her research interests include resource management and performance analysis in wireless networks and space networks.

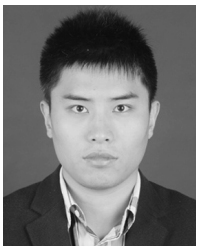

WEIHUA WU received the B.S. and M.E. degrees in telecommunications engineering and the Ph.D. degree in communication and information systems from Xidian University, China, in 2011, 2014, and 2017, respectively. From 2016 to 2017, he was a Visiting Student with the University of Avignon, France. He is currently a Lecturer with the State Key Lab of ISN, Xidian University. Since March 2019, he has also been with the Singapore University of Technology and Design as a Visiting Scholar sponsored by the China Scholarship Council (CSC). His research interests include wireless resource allocation, and stochastic network optimization and their applications in LTE-U networks.

QINGHAI YANG received the B.S. degree in communication engineering from the Shandong University of Technology, China, in 1998, the M.S. degree in information and communication systems from Xidian University, China, in 2001, and the Ph.D. degree in communication engineering from Inha University, South Korea, in 2007, with university-president award. From 2007 to 2008, he was a Research Fellow with UWB-ITRC, South Korea. Since 2008, he has been with Xidian University, where he is currently a Professor. His current research interests include the fields of autonomic communication, content delivery networks, and LTE-A techniques.

DI ZHOU received the B.E. degree in information engineering and the Ph.D. degree in communication and information systems from Xidian University, Xi'an, China, in 2013 and 2019, respectively. She was a Visiting Ph.D. Student with the Department of Electrical and Computer Engineering, University of Houston, from 2017 to 2018. Since 2019, she has been with the State Key Lab of ISN, School of Telecommunications Engineering, Xidian University, where she currently holds a faculty postdoctoral position. Her research interests include routing, resource allocation, and mission planning in space information networks.

WENZHU ZHANG received the B.S., M.S., and Ph.D. degrees in communications engineering from Xidian University, Xi'an, China, in 1994, 1999, and 2004, respectively. From 2005 to 2006, he was a Research Associate with the Illinois Institute of Technology, Chicago, IL, USA, where he was responsible for the development in research of new radio access technology. From 2012 to 2013, he was a Postdoctoral Researcher with Inha University, Incheon, South Korea. He is currently a Professor with the School of Information and Control Engineering, Xi'an University of Architecture and Technology. His research interests include the field of ad hoc wireless networks, network performance analyzing, and cognitive radio networks.